Roof Edge Detection by Mathematical Morphology†

Jin–Chang Cheng‡
Hon–Son Don
Department of Electrical Engineering
State University of New York
Stony Brook, NY 11794

Abstract

This paper presents a new method for roof edge detection. In practice, digital images are noise contaminated. A simple method of roof edge detection is to smooth the noisy image, take its derivative, and then use step edge detection techniques to detect roof edges. However, reducing noise by smoothing will also blur the edges since edges correspond to the high frequencies as noises do. Our method is to classify roof peaks from noise peaks by morphological testing. Roof edges on digital images are found by looking for the leaf nodes of the skeletal tree. A leaf node represents a local maximum (or peak). The size of subtree containing the leaf node is tested to distinguish the noise from the roof edge. The skeletal trees of gray scale images can be easily found by gray scale morphological skeleton operations.

Keywords: Roof edge detection, skeletal tree, mathematical morphology, image Processing

1. Introduction

The segmentation problem is defined as partitioning the image into segments. It is an intrinsic part of an image understanding system. Boundaries are one of the basic sorts of segments to extract. If the boundary of an object can be extracted successfully then the scene analysis can be simplified and recognition becomes highly feasible. The boundary is composed of edge segments and thus edge detection plays an important role in low-level image processing. In images, any type of significant scene structure appear as discontinuities in the gray value (intensity or range), generally called edges. There are at least two types of edges that are important in image analysis: jump (or step) edge and roof edge. In Fig. 1, we observe 2-D instances of jump edges and roof edges. For intensity images, jump edge is defined as the boundary between two regions whose brightness values are significantly different, and usually corresponding to occluding boundary of objects in a scene. As in intensity images, jump edges in range images are formed where depth values are discontinuous. Such edges occur when an object occludes another object or when part of an object occludes itself. Here, roof edge includes crease edge and ridge edge. A crease edge occurs on a crease line which is the intersection of two planes. A crease line is a straight line consisting of a series of crease points. As we walk along the crease line the points to the right and left of us are lower than the ones we are on. A crease edge occurs where there is a local maximum in one direction. A ridge edge is identical to a crease edge except it is the intersection of two non-planar surfaces. The ridge line may be flat, sloped upward, sloped downward, curving upward, or curving downward.

Most work on edge detection has been focused on jump edge detection. Roof edge detection has received relatively less attention. One possible reason may be due to the fact that identification of roof edges is a particularly difficult problem than that of jump edges. Our main interest in this paper is with the detection of roof edges using morphological operations.

Theoretically, any jump edge detectors can be used to detect roof edges by taking the smoothed derivative (or gradient) of the image. However, a problem with the gradient vector estimation is the need to define a neighborhood. There will be distortion of the "true" gradients in the vicinity of roof edges, so that gradients will not be wholly discontinuous in traveling over an edge but will gradually change. Also smoothing may destroy edge details. Consider the

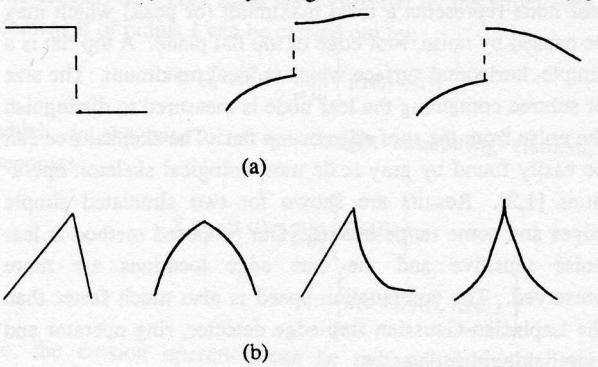

Fig. 1: (a) Jump edges, (b) roof edges.

†This work was supported by the U.S. National Science Foundation under Grant IRI-8710856 and U.S. Army Research Office under Contract DAAL 0338K0033.
‡Present address: Center for Optics, New York Institute of Technology, 100 Glen Cove Avenue, Glen Cove, NY 11542

Laplacian-Gaussian jump edge detector which will take the derivative twice. Then the gradient method needs to take the derivative three times in total. For each derivative operation, the operating window will be enlarged and thus the locality of the roof edge detector will not be good. Moreover, taking the derivative too many times may enhance the noise, resulting in many spurious edges.

Most approaches involve applying a local operator to the neighborhood of every pixel to determine which pixels have a "roof" quality [4, 5, 7, 9]. These kind of approaches are usually very sensitive to noises. Inokuchi, et al [5] proposed a pixel classification method, called ring operator, to classify pixels into jump edge, roof edge and plane in range images. It transforms a set of pixels on a ring placed on observed point into frequency domain. A pixel is classified as a roof edge pixel if the amplitude of the second component is sufficient "large" (than a preset threshold t_2) and the first and the third components are fairly small (than another two preset thresholds t_1 and t_3). Haralick [4] proposed fitting the image with two-variable cubic polynomial. Ridges are marked at pixels by looking for zero crossings of the first directional derivative taken in a direction which extremizes the second directional derivative.

Mathematical Morphology is an approach to image processing based on set theoretic concepts of shape. Serra [10] defined a ridge detector by upper thinnings. The upper thinnings is complicated and does not have an explicit representation. Basically, it is derived from the Hit-Miss transformation. The Hit-Miss transformation required two disjoint structuring elements. Serra provided a guide to the selection of structuring elements; however, a hexagonal grid are employed, which makes the presentation difficult to interpret. Recently, Noble [8] proposed a morphological ridge detector by the set difference of the closing and opening of the image surface by a spherical structuring element. Noble's detector is very simple but very sensitive to noise.

In this paper, we propose a roof edge detector by using mathematical morphology. Roof edges on digital images are found by looking for the leaf nodes of the skeletal tree. A leaf node represents a local maximum (or peak) which may be caused by noise, roof edge or top flat plane. A top flat is a simple, horizontal surface which is local maximum. The size of subtree containing the leaf node is measured to distinguish the noise from the roof edge or top flat. The skeletal tree can be easily found by gray scale morphological skeleton operations [1,2]. Results are shown for two simulated simple edges and some range images. Our proposed method is less noise sensitive and the true edge locations are more preserved. The computation speed is also much faster than the Laplacian-Gaussian step-edge detector, ring operator and Haralick's ridge detector.

2. Review of Simple Morphological Edge Detectors

In this section, we review some simple morphological edge detectors. Roof edges, jump edges and sharp corners are similar entities as far as a morphological operator is concerned, for in all cases the operator responds to the suddenly discontinuities of gray scale values in the image. Several simple morphological corner and step edge detectors are proposed in [3,6], which include

(1) Erosion residue operator ($f - f \ominus_g B$);

(2) Dilation residue operator ($f \oplus_g B - f$);

(3) Combinations (maximum, minimum, or summation) of (1) and (2); and

(4) Blur and minimum operator ($\min \{ f_1 - f_1 \ominus_g B, f_1 \oplus_g B - f_1 \}$),

where f_1 is the result of the input image f with a blurring operation.

The results of the above operators are the images of edge strength. An appropriate threshold value is, then, selected to threshold the edge strength image into a binary edge image. Although these detectors are simple, (1)-(3) are shown to be noise sensitive and/or position biased [6]. Despite their noise sensitivity, there are some other reasons that (1)-(4) are not suitable for the roof edge detection. For example, given an ideal roof edge shown in Fig. 2a and a spherical structuring element in Fig. 2b. The application of the erosion residue operator on the ideal roof edge get the result edge strength shown in Fig. 2c. Obviously, Fig. 2c shows that this operator fails to detect the ideal roof edge.

Recently, Nobel[8] proposed a morphological roof and corner detector by the set difference ($f \bullet_g B - f \circ_g B$) of the closing and opening of the image. The opening operation can be visualized as rolling the structuring element under the top surface and only keeping points where the structuring element touches the surface. The dual operation of closing rolls the structuring element over the complement of the umbra of the surface. To test its performance, we apply Nobel's roof edge detector to a computer-generated roof edge profile, shown in Fig. 3a, which consisting of two ideal roof edges of

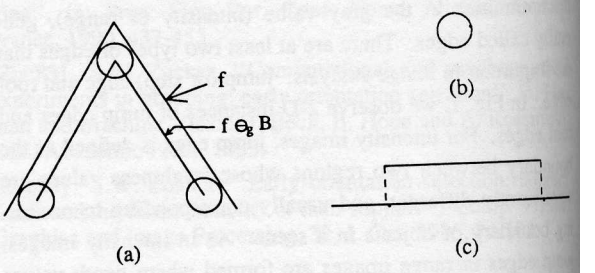

Fig. 2: Application of the erosion residue operator on (a) the ideal roof edge by using (b) spherical structuring element, (c) result of the operation.

different "sizes". Fig. 3c shows the result. We see that this detector has better response on sharper corner. Fig. 3b is obtained by adding zero-mean Gaussian noise with standard deviation 15 to the ideal roof edges shown in Fig. 3a. The result of Nobel's operator applied on Fig. 3b is shown in Fig. 3d. As we can see from Fig. 3d, this detector is also sensitive to noise.

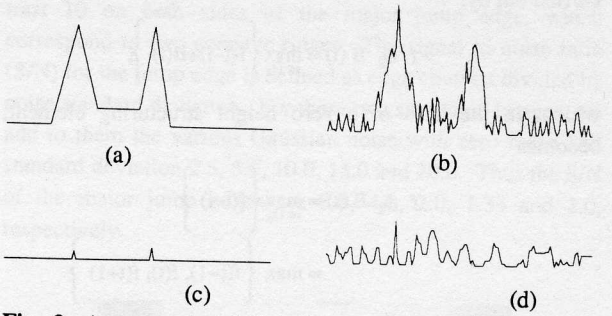

Fig. 3: An example of Nobel's roof-edge detector: (a) an ideal roof edge profile, (b) noise contaminant of (a), (c) and (d) show respective results of Nobel's operator on (a) and (b).

3. A New Morphological Ridge Detector

As discussed in the previous section, the simple morphological detectors based on erosion residue, dilation residue or difference of closing and opening either are sensitive to noise or have poor localization. In this section we propose an algorithm for ridge edges detection, which is less noise sensitive. The algorithm is based on the skeletal trees of the gray scale image which is provided by the gray scale morphological skeleton transformation.

3.1. Skeletal Tree

The skeletal trees of a waveform are composed of the skeleton points of the waveform. A node on the skeletal tree is a skeleton point associated with its radius as the attribute. Skeleton points can be generated by using gray scale morphological skeleton transformation [1,2]. The following is a summary of properties of the skeletal tree :

(1) Each peak on the waveform will correspond to a leaf node which is the smallest radius in the subwaveform. A subwaveform is defined as the subset of the waveform contains a peak and the portion between its two neighboring valleys. A subwaveform is labeled with its corresponding peak. Fig. 4a shows three subwaveforms S_1, S_2 and S_3 .

(2) Every node has a single parent. Most nodes have only one son, but some nodes may have more than one sons.

(3) Parent node always has radius greater than or equal to its son nodes. Numbers shown in Fig. 4b indicate the corresponding radius at each node. Node Q is, of radius 9, a parent node of nodes P_1 and P_2 which are of radius 4 and 2, respectively.

(4) The nearest common predecessor of two nodes corresponds to a valley on the waveform. Fig. 4b shows node Q, which has two son nodes P_1 and P_2, corresponding to a valley between subwaveform S_1 and subwaveform S_2.

(5) The original waveform can be easily reconstructed from its skeletal tree by using inverse gray scale morphological skeleton transformation [1,2].

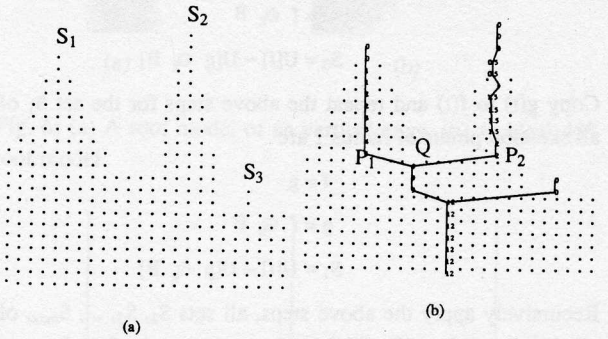

Fig. 4: (a) A waveform with three subwaveforms, (b) skeletal tree of waveform (a).

3.2. The Construction of Skeletal Tree

The Construction of skeletal tree is briefly described in this section. We apply the one-dimensional gray scale skeleton transformation to the waveform with a fixed unit sized structuring element. The domain of the structuring element B of radius 1 is defined by the set

$$D_B = \{-1, 0, 1\}$$

and B(t), $t \in D_B$, is zero. The gray scale skeleton transformation [1,2] needs two kinds of morphological operations: erosion and opening. Morphological gray scale opening is performed by gray scale erosion followed by gray scale dilation. The erosion of a gray scale waveform f(t) by the structuring element B of radius 1 can be carried out by:

$$f \ominus_g B(t) = \min_{i \in D_B} \{ f(t+i) - B(i) \},$$

which, in the case of a zero height structuring element, becomes

$$f \ominus_g B(t) = \min_{i \in D_B} \{ f(t+i) \}$$
$$= \min \{ f(t-1), f(t), f(t+1) \}$$

So, the erosion operation can be reduced to finding the minimum of three numbers. The dilation of a gray scale waveform f(t) by the structuring element B of radius 1 can be

carried out by:

$$f \oplus_g B(t) = \max_{i \in D_B} \{ f(t-i)+B(i) \},$$

which, in the case of a zero height structuring element, becomes

$$f \oplus_g B(t) = \max_{i \in D_B} \{ f(t-i) \}$$

$$= \max \{ f(t-1), f(t), f(t+1) \}$$

The dilation operation can be achieved by finding the maximum of three numbers.

We find $f \ominus_g B$ first, and save it as g(t) for later use, then the set S_0 of all skeleton points of zero radius are

$$g = f \ominus_g B$$

$$S_0 = U[f] - U[g \circ_g B]$$

Copy g(t) to f(t) and repeat the above steps for the set S_1 of all skeleton points of radius 1 are

$$f = g$$

$$g = f \ominus_g B$$

$$S_1 = U[f] - U[g \circ_g B]$$

Recursively apply the above steps, all sets S_2, S_3, ..., S_{maxr} of all skeleton points of radii from 2 to *maxr* can be found.

Note that each step generates all skeleton points of the same radius. Two skeleton points of the same radius may be 'close' to each other. That means the skeleton may be, at most, of width two. This is due to the shape of the structuring element we choose. Also, skeleton points of the same radius within a subwaveform must have the same t value (or t and t+1 in the case of width two) and therefore, their plots form a (or two, at most) vertical line segment. In the real implementation, those skeleton points with same t value can be saved as only one tree node, in the case of width 1. In the case of width two, we combine these two 'close' skeleton points into one with radius one half more. That is, let $P_1 = (r, t_1)$ and $P_2 = (r, t_1+1)$ be two 'close' skeleton points of radius r at $t=t_1$ and t_1+1, respectively, then we combine them into one point $P = (r+0.5, t_1+0.5)$ with radius r+0.5 at $t=t_1+0.5$.

After all skeleton sets S_i are found, the construction of the skeletal tree is simple. The parent-son relationship is built as follows. Remember that the nodes of the skeletal tree are the skeleton points of different sizes. Let $P = (r, t_1) \in S_r$ and $Q = (r+1, t_2) \in S_{r+1}$ be any two skeleton points of radius r and r+1, respectively. (Note that, in the case of skeleton points of radius r+0.5 exist, we consider skeleton points of radii r and r+0.5 first, then those of r+0.5 and r.) Then node P is a son node of Q, if and only if

$$|t_2 - t_1| \leq r+1.$$

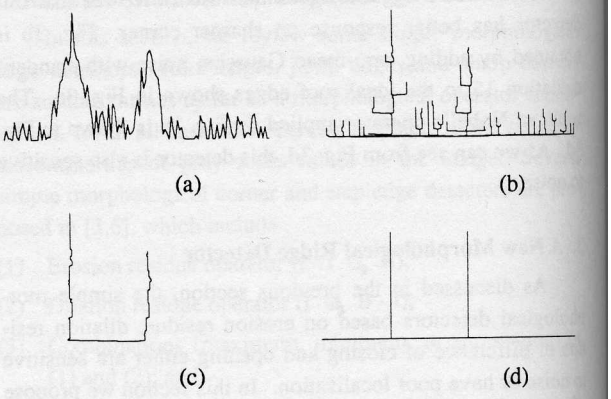

Fig. 5: (a) Same as Fig. 3b, (b) skeletal tree of (a), (c) result after removing noise peaks, (d) two roof edge locations are found.

Similarly, every points in S_0 is naturally a leaf node and all nodes which have no sons are leaf nodes. Leaf nodes are particularly interested since they are candidates of ridge points. Ridge point detection is our major concern in this paper.

3.3. Roof Edge Detection

Every leaf node in the skeletal tree corresponds to a peak (local maximum). Roof edges and top flats are local maxima; so they are peaks in the waveform. They can be located from the leaf nodes of the skeletal tree. The difference between them is the radius associated with the leaf node. Roof edges associate with small radius and top flat large radius. The size depends on the resolution of the picture. However, not every leaf node corresponds to roof edge or top flat, since noise may generate peaks too. The noise subwaveforms must be small compared with the roof or top flat subwaveforms. To distinguish between 'small' subwaveforms and 'large' subwaveforms, we set a threshold value T. The decision then becomes very simple, since most nodes have only one son. Those nodes, which have more than one sons, must be corresponding to more than two subwaveforms (or two peaks). If one son node P_1 is of radius less than T and the other son node P_2 is of radius greater than or equal to T, we claim that node P_1 corresponds to a noise peak. Therefore the whole subtree rooted by node P_1 must be removed. On the other hand, if both node P_1 and node P_2 are of radius less than T, then both nodes may correspond to two noise peaks or one node corresponds to a roof peak and the other node a noise peak but close to the roof peak. In such case, we check the difference between the radius of node P_1 (or P_2) and the radius of their parent node Q. If this difference is large (more than 3 in our implementation), then both node P_1 and node P_2 must be noises. Otherwise, one of them is a roof peak and the other is a noise peak which is close to the roof. In such case, a heuristic decision is made by remov-

ing the one with smaller gray scale value. Fig. 5 demonstrates steps of this roof edge detector. Fig. 5b shows the skeletal tree of Fig. 5a, which is the same as Fig. 3b. Fig. 5c shows the result after the small branches, which correspond to noise peaks, are trimmed. From Fig. 5c, we see that there are only two leaf nodes left, which corresponding to the original roof edge pixels and the result is shown in Fig. 5d.

3.4. Computational Complexity

Since the threshold T determines the acceptance of a subwaveform as a roof subwaveform or the rejection as a noise subwaveform. Any subwaveform has size greater than or equal to T will not be a noise subwaveform. Therefore, the skeleton set $\{S_i\}$, $0 \le i \le maxr$, only needs to be calculated up to $maxr = T$. In all the experiments, which will be described in next section, T=10 is large enough. The time complexity analysis is similar to that described in [1,2], since the computation time in this roof edge detection algorithm is basically dominated by the skeletonization process. As analyzed in Section 3.3.1, the skeletonization process of raster scan fashion (1-D) takes (T^2+5T+2) parallel min/max operations on a parallel machine, or, about $(T^2+5T+2)\cdot N^2$ operations on a conventional sequential machine for image of size $N \times N$ pixels.

4. Experimental Results

In this section, we present some experimental results to show the performance of our morphological roof edge detection algorithm. We used two simulated roof images and three range images for the experiments. For the purpose of comparison, the images in all experiments were processed by applying 1) our algorithm, 2) Differential-Laplacian-of-Gaussian (DLOG) edge detector, (3) cubic facet ridge detector (Haralick [4]), and (4) ring operator (Inokuchi, et al [5]). The Differential-Laplacian-of-Gaussian (DLOG) edge detector is implemented by taking the first order difference along its gradient direction and then apply the Laplacian-of-Gaussian (LOG) edge detector. The ring operator can classify pixels into jump edge, roof edge and plane in range images. We use it for the detection of only roof edges. Before running the ring operator, there are three thresholds must be set. We have run the ring operator for several different sets of thresholds and only the best results will be shown.

The first simulated image is an ideal vertical roof edge, shown in Fig. 6(a), which has slope +10 (in pixel unit) in one side and -10 in the other side. The size of the image is 128 by 128 pixels. The second image, shown in Fig. 6(b), simulates an ideal 45° roof edge which is obtained by 45° rotation of Fig. 6(a). If we take the differential operation on the first image, the result will have an ideal major jump edge with edge contrast 20 plus two minor jump edges with edge contrast 10 on both sides of the major jump edge, which correspond to two concave ridges. The signal to noise ratio (S/N) for the jump edge is defined as edge contrast divided by noise standard deviation. For these two simulated images, we add to them the various Gaussian noise with zero mean and standard deviation 2.5, 5.0, 10.0, 15.0 and 20.0. Thus the S/N of the major jump edges are 8.0, 4.0, 2.0, 1.33 and 1.0, respectively.

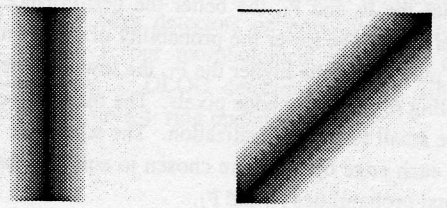

(a) (b)

Fig. 6: (a) A roof model of an vertical edge, (b) an ideal 45° roof model.

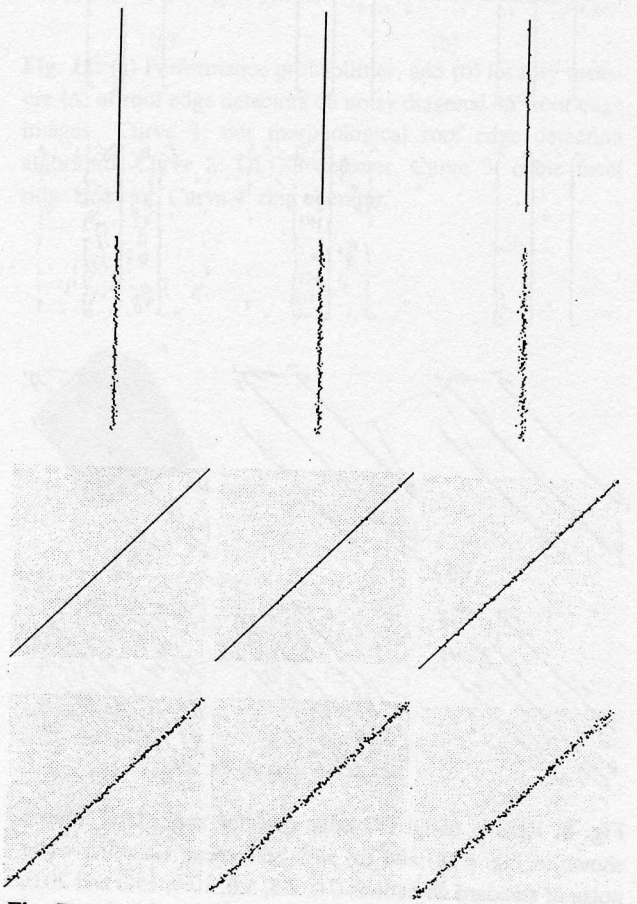

Fig. 7: Results of our roof edge detection algorithm applied on images shown in Fig. 6 (a) and (b) with zero mean Gaussian white noise of standard deviations 0.0, 2.5, 5.0, 10.0, 15.0 and 20.0, respectively (cpu time ≈ 18 sec.)

To evaluate the performance of different roof edge operators, we use (1) the conditional probability of the label edge* given the true edge P_0=Prob(L | E)**, where L is the set of the label edges and E is the set of the true edges, (2) the conditional probability of the true edge given the label edge P_1=Prob(E | L)***, and (3) mean distance (Δ) of label edge pixels to the the center of the true edge. The measurements of P_0 and P_1 indicate 'how good the detection is' and the measurement of Δ indicates 'how good the localization is'. The higher the P_0 and P_1, the better the performance. Since the higher the P_0, the lower the probability of falsely marking nonedge pixels; and the higher the P_1, the lower the probability of failing to mark real edge pixels. The measurement of Δ should be small for good localization. The adjustable parameters for each edge operator are chosen to equalize these two conditional probabilities P_0 and P_1.

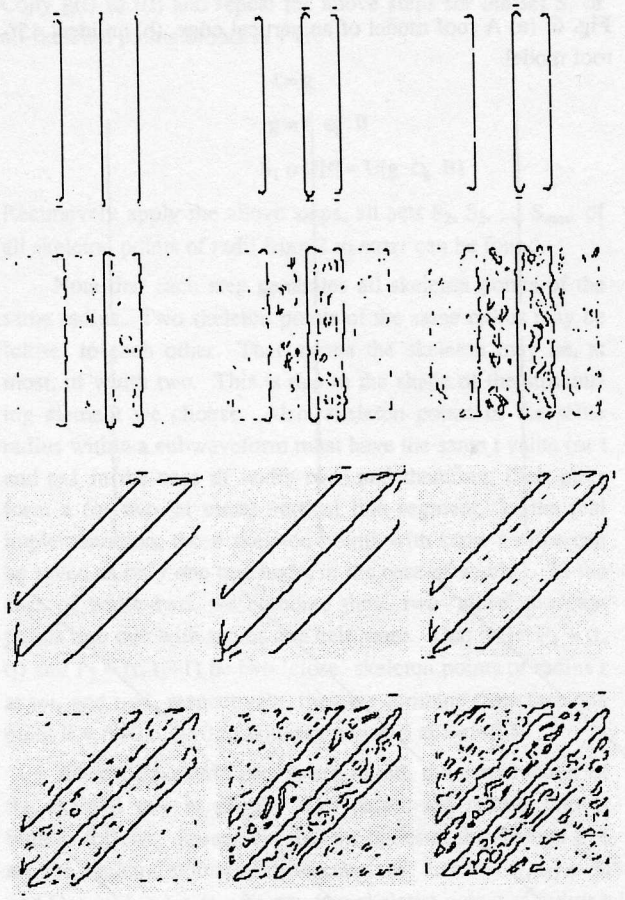

Fig. 8: Results of DLOG edge detector applied on images shown in Fig. 6 (a) and (b) with zero mean Gaussian white noise of standard deviations 0.0, 2.5, 5.0, 10.0, 15.0 and 20.0, respectively (cpu time ≈ 1030 sec.)

*label edge is referred to the pixel acclaimed to be edge pixel by the edge detector.
**P_0 is approximated by $n(E \cap L)/n(E)$, where $n(S)$ is the cardinal number of the set S.
***Similarly, P_1 is approximated by $n(E \cap L)/n(L)$.

The DLOG detector responds to convex roof edges as well as concave roof edges. Therefore, when calculating the probabilities P_0 and P_1, the set E of true edges for this detector will include both convex roof edge pixels and concave roof edge pixels. Our morphological roof edge detector responds to convex roof edges only. The set E will only includes convex roof edge pixels in the evaluation of our algorithm. To detect the concave roof edges, our algorithm can be easily modified based on the dual properties of morphological operations (erosion duals to dilation and opening duals to closing).

Fig. 7 shows a sequence of edge images which are the results of applying our algorithm to the two simulated images with zero mean Gaussian white noise of standard deviations 0.0, 2.5, 5.0, 10.0, 15.0 and 20.0. Fig. 8, 9, and 10 show the corresponding parts of DLOG edge detector, cubic facet ridge detector, and ring operator, respectively. Those edge detectors are implemented in C language on VAX-11/780. The computation time (user time plus system time) of our algorithm for each image is about 18 seconds. That of DLOG

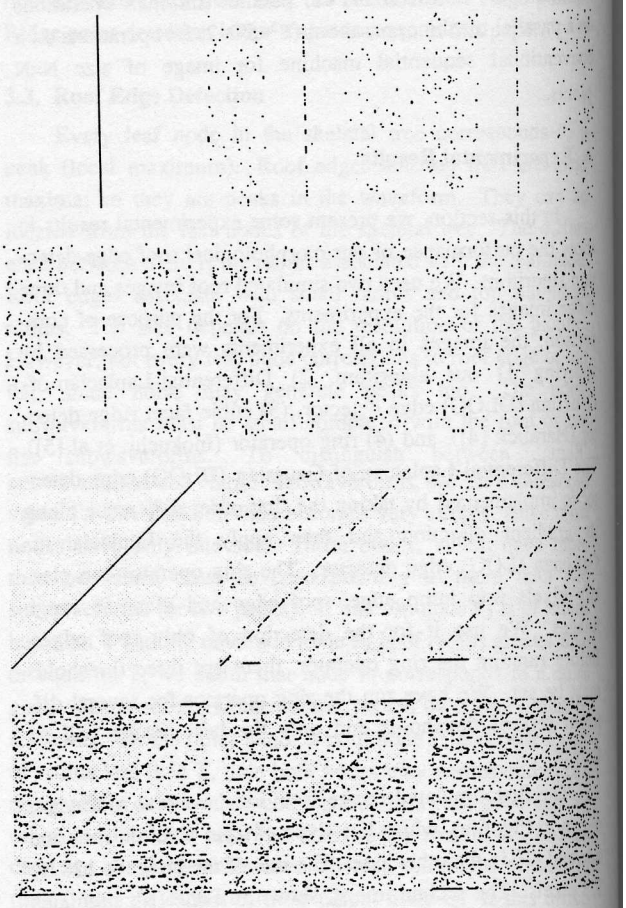

Fig. 9: Results of cubic facet ridge detector (Haralick [4]) applied on images shown in Fig. 6 (a) and (b) with zero mean Gaussian white noise of standard deviations 0.0, 2.5, 5.0, 10.0, 15.0 and 20.0, respectively (cpu time ≈ 263 sec.)

algorithm is about 1030 seconds, cubic facet algorithm 263 seconds, and ring operator 42 seconds. Fig. 11 and Fig. 12 show the performance plots of those detectors. To suppress image border effects, the performance probabilities P_0 and P_1 are measured in a window of size 100×100. The locality (Δ) are measured in the neighborhood of the ideal roof edge with distance half way to the two minor edges. The results show that our algorithm have much better performance than the other edge detectors. The DLOG operator produces thick edge lines and lots of false edge pixels. Cubic facet ridge detector and ring operator have good results when the noise is small.

Finally, we illustrate by using examples of applying our algorithm to three range images. The images are shown in Fig. 13 (a), Fig. 14 (a) and Fig. 15 (a), respectively. We apply our algorithm, the cubic facet ridge detector and the ring operator to these images. The resulting edge images are shown in Fig. 13 (b)-(d), Fig. 14 (b)-(d) and Fig. 15 (b)-(d), respectively. A visual evaluation leaves the impression that our algorithm has the best performance.

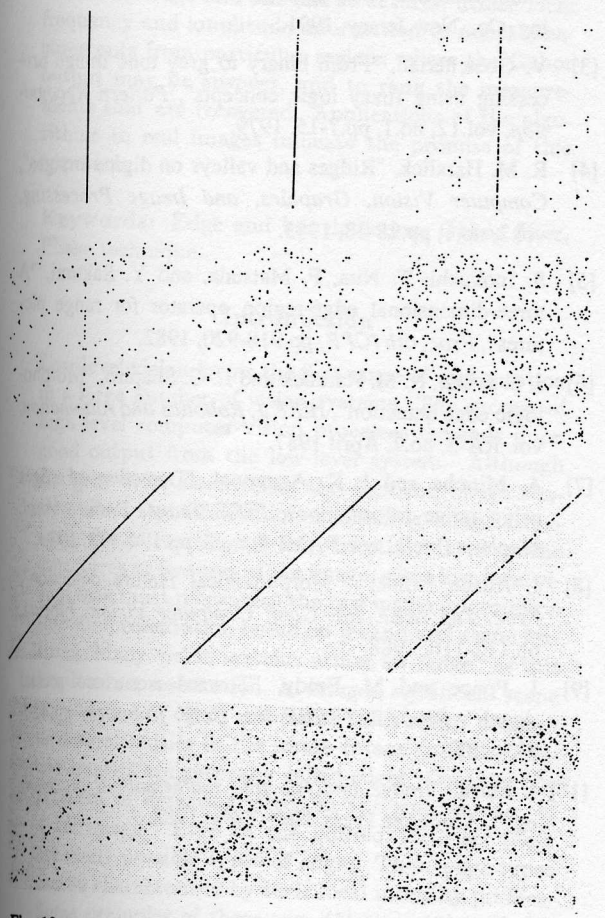

Fig. 10: Results of ring operator (Inokuchi, et al [5]) applied on images shown in Fig. 6 (a) and (b) with zero mean Gaussian white noise of standard deviations 0.0, 2.5, 5.0, 10.0, 15.0 and 20.0, respectively (cpu time ≈ 42 sec.)

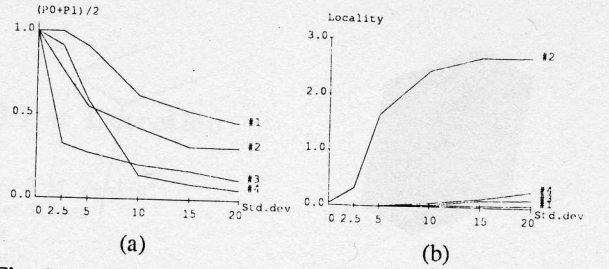

Fig. 11: (a) Performance probabilities, and (b) locality measure (Δ) of roof edge detectors on noisy vertical roof edge images. Curve 1: our morphological roof edge detection algorithm, Curve 2: DLOG detector, Curve 3: cubic facet ridge detector, Curve 4: ring operator.

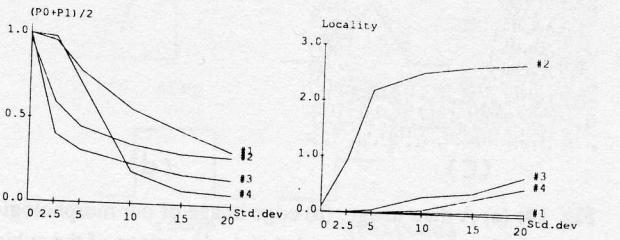

Fig. 12: (a) Performance probabilities, and (b) locality measure (Δ) of roof edge detectors on noisy diagonal 45° roof edge images. Curve 1: our morphological roof edge detection algorithm, Curve 2: DLOG detector, Curve 3: cubic facet ridge detector, Curve 4: ring operator.

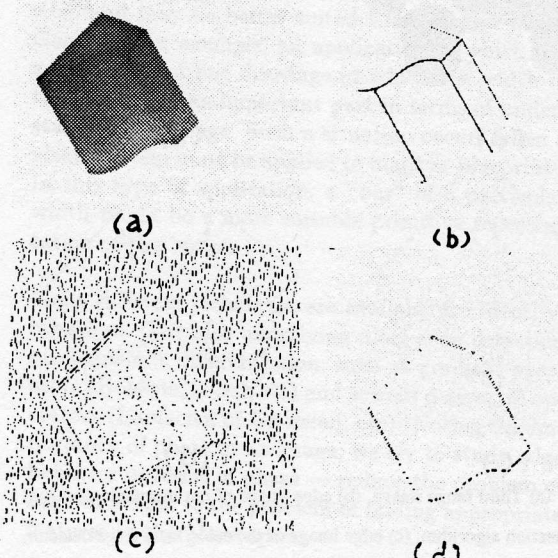

Fig. 13: (a) A bench chair image, (b) edge image of our morphological roof edge detection algorithm, (c) edge image of the cubic facet ridge detector, (d) edge image of the ring operator.

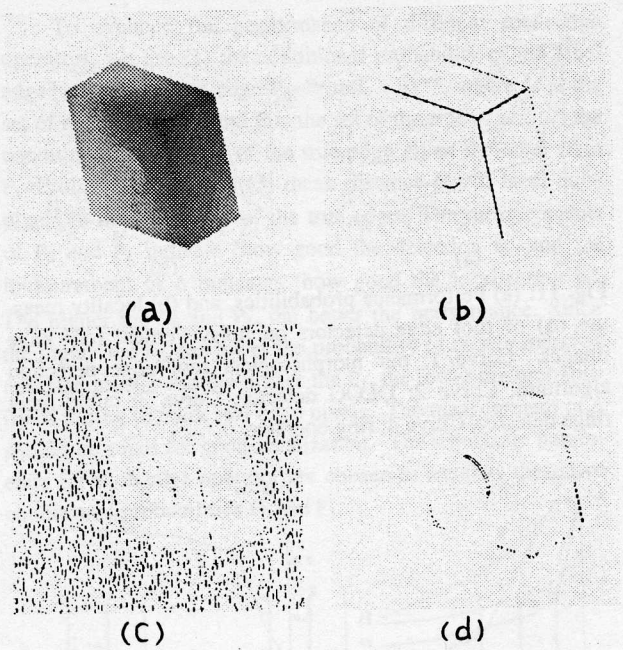

Fig. 14: (a) A dice image, (b) edge image of our morphological roof edge detection algorithm, (c) edge image of the cubic facet ridge detector, (d) edge image of the ring operator.

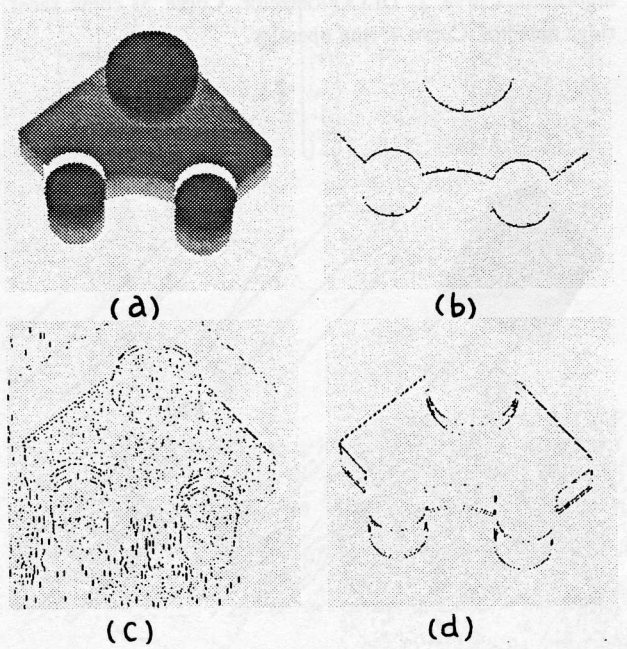

Fig. 15: (a) Third range image, (b) edge image of our morphological roof edge detection algorithm, (c) edge image of the cubic facet ridge detector, (d) edge image of the ring operator.

5. Conclusions

We have proposed a roof edge detection algorithm based on the mathematical morphology. Roof edges on digital images are detected by looking for the leaf nodes of the skeletal tree. A leaf node represents a local maximum (peak) in the image. The size of subtree containing the leaf node is tested to distinguish the noise from the roof edge. The skeletal trees of gray scale images can be obtained by applying the gray scale morphological skeleton operations. Experimental results show that this algorithm is faster and has better performance than many other methods.

References

[1] J. C. Cheng and H. S. Don, "Segmentation of Bilevel Images Using Mathematical Morphology", *Proc. of Vision Interface* pp.142-149, May 1990.

[2] J. C. Cheng and H. S. Don, "Segmentation of Bilevel Images: A Morphological Approach" *Pattern Recognition: Algorithms, Architectures and Applications*. ed. R. Plamondon and H. D. Cheng, World Scientific Publishing, Co., New Jersey, 1991.

[3] V. Goetcherian, "From binary to grey tone image processing using fuzzy logic concepts", *Pattern Recognition*, vol.12, no.1, pp.7-15, 1979.

[4] R. M. Haralick, "Ridges and valleys on digital images", *Computer Vision, Graphics, and Image Processing*, vol.2, no.1, pp.28-38, 1983.

[5] S. Inokuchi, T. Nita, F. Matsuda, and Y. Sakurai, "A three-dimensional edge-region operator for range pictures", *Proc. 6th ICPR*, pp.918-920, 1982.

[6] J. S. J. Lee, R. M. Haralick and L. G. Shapiro, "Morphologic edge detection", *IEEE J. Robotics and Automation*, vol. RA-3, no.2, April 1987.

[7] A. Mitiche and J. K. Aggarwal, "Detection of edges using range information", *IEEE Trans. Pattern Anal. Machine Intell.*, vol. PAMI-5, no.2, pp.174-178, 1983.

[8] J. Alison Noble, " Morphological feature detection", *Proc. 2nd IEEE Int. Conf. Computer Vision*, Florida, pp.112-116, 1988.

[9] J. Ponce and M. Brady, "Toward a surface primal sketch", *Proc. 2nd IEEE Int. Conf. Robotics*, pp.420-425, 1985.

[10] J. Serra, *"Image analysis and mathematical morphology"*, Academic Press, New York, 1982.